

# Potential-driven eddy current in rippled graphene nanoribbons

Hua-Tong Yang\*

*Key Laboratory for UV-Emitting Materials and Technology of Ministry of Education,  
Department of Physics, Northeast Normal University, Changchun 130024, China*

It is well known that an eddy current will be induced in a conductor subject to a varying magnetic field. Here we propose another mechanism of generating nano-scale eddy current in rippled graphene nanoribbons(GNRs), which is only driven by an electric potential. In particular, it is found that under appropriate gate voltages, a local deformation may induce some unexpected global eddy currents, which form vortices in both rippled and entire flat areas of the GNR. We will explain that these vortices in flat areas is a manifestation of the nonlocality of quantum interference.

## A. Introduction

Graphene, as the first experimentally available strictly two-dimensional crystal[1, 2], has offered a lot of new possibilities for both fundamental research and new technologies due to its exceptional mechanical and electronic properties[3–5]. These single-atom-thick carbon membranes are very soft and flexible. Experiments have observed that graphene sheets are rippling even in free-standing condition[6–8]. This feature is expected to have significant influences on their electronic properties and to result in some new observable effects[9–12]. Recently, Bao et al. reported a method to control and create nearly periodic ripples of sinusoidal form in graphene sheets[8], which provides a possibility to design and manipulate electronic states in graphene sheets by controlling their local structure. According to the continuous model, a linear approximation of the tight-binding Hamiltonian in vicinity of its Dirac points, the electronic states of graphene can be described by a massless Dirac equation. In this model the action of a ripple can be represented by an effective vector field[13–15], which essentially is the shift of the Dirac points due to the deformation, and a velocity tensor representing anisotropy of the energy band[16]. This continuous model is adequate if the deformation is very smooth. However, this condition cannot be always satisfied in realistic graphene sheets, since some corrugations in graphene sheets are not so smooth.

In this work, the local density of states(LDOS) and current flow in rippled GNRs are investigated by using the tight-binding model and non-equilibrium Green's function(NEFG) method[17–19]. It is found that the current distributions near each step edge of the conductance staircases are unstable, they will become non-potential or eddy flows if the GNRs are rippled, although their driven force is potential. In particular, there also occur some global eddy currents, which are still vortical in the flat regions of the GNRs. The vortices in flat areas is rather exotic from the classical view point, because there is no local deflection mechanism in these areas. We will explain that this phenomenon is originated from a non-local

quantum interference effect. This eddy current will give rise to a very inhomogeneous magnetic field in nanometer scale. It not only has crucial influences on the performance of graphene-based electronic devices and circuits, but may also have important potential applications.

## B. Model and Method

The electronic properties of graphene can be described by the nearest tight-binding Hamiltonian

$$\hat{H} = \sum_{\langle \mathbf{r}, \mathbf{r}' \rangle} t(\mathbf{r} - \mathbf{r}') c^\dagger(\mathbf{r}) c(\mathbf{r}') + \text{H.c.} \quad (1)$$

where  $\mathbf{r}, \mathbf{r}'$  denote two nearest lattice points,  $c^\dagger, c$  are electron's creation and annihilation operators,  $t(\mathbf{r} - \mathbf{r}')$  is a distance-dependent hopping amplitude modeling the influence of deformation and can be fitted by

$$t(\mathbf{r} - \mathbf{r}') \simeq t_0 e^{\alpha(1-|\mathbf{r}-\mathbf{r}'|/l)}, \quad (2)$$

where  $t_0 = -2.75\text{eV}$ ,  $\alpha \simeq 3.37$ ,  $l \simeq 1.42\text{\AA}$ [20, 21]. For the tight-binding model, we define the bond current  $j(\mathbf{r}, \mathbf{r}')$  from  $\mathbf{r}$  to  $\mathbf{r}'$  by the conservation equation  $\sum_{\mathbf{r}'} j(\mathbf{r}, \mathbf{r}') = -\frac{\partial \langle \hat{n}(\mathbf{r}t) \rangle}{\partial t}$ , where  $\hat{n}(\mathbf{r}t) = 2c^\dagger(\mathbf{r}t)c(\mathbf{r}t)$  is the electronic number operator, the factor 2 comes from the spin degree of freedom. From the equation of motion we have

$$j(\mathbf{r}, \mathbf{r}', t) = \frac{4}{\hbar} \text{Re}[t(\mathbf{r} - \mathbf{r}') G^<(\mathbf{r}'t, \mathbf{r}t)], \quad (3)$$

where  $G^<(\mathbf{r}'t', \mathbf{r}t) = i\langle c^\dagger(\mathbf{r}t)c(\mathbf{r}'t') \rangle$  is the lesser Green's function. In steady states, the current can be written as  $j(\mathbf{r}, \mathbf{r}') = \int j(\mathbf{r}, \mathbf{r}', E) dE$ , where

$$j(\mathbf{r}, \mathbf{r}', E) = \frac{4}{\hbar} \text{Re}[t(\mathbf{r} - \mathbf{r}') G^<(\mathbf{r}', \mathbf{r}, E)] \quad (4)$$

is the current per unit energy[22].

For the sake of simplicity, we only consider zigzag and armchair GNRs with a finite rippled region. The ripple is a static height fluctuation given by

$$z(\mathbf{r}) = \begin{cases} h \sin(\mathbf{k} \cdot \mathbf{r} + \phi_0), & 0 \leq \mathbf{k} \cdot \mathbf{r} \leq 2m\pi \\ h \sin \phi_0, & \mathbf{k} \cdot \mathbf{r} < 0 \text{ or } \mathbf{k} \cdot \mathbf{r} > 2m\pi, \end{cases} \quad (5)$$

\*Electronic address: yanght653@nenu.edu.cn

with  $\phi_0$  an arbitrary constant and  $m$  an integer, the atomic in-plane displacement is ignored. A typical configuration of the rippled GNRs considered in this paper is shown in Fig.1.

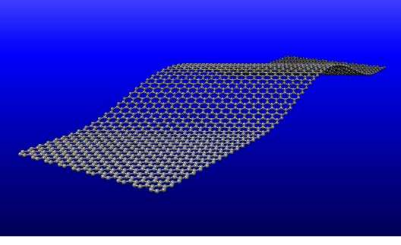


FIG. 1: An  $N = 20$  zigzag GNR with a sinusoidal ripple given by Eq.(5), here  $h \simeq 2a$  with  $a \simeq 2.46\text{\AA}$  the length of the basis vectors, the ripple wavelength  $\lambda = 30a$ , the included angle  $\theta_{\mathbf{k}}$  between the GNR axis and  $\mathbf{k}$  is  $30^\circ$ ,  $\phi_0 = -\pi/2$ ,  $m = 1$ .

In order to calculate the LDOS and current of GNRs by using the NEFG method[17–19], the GNRs have to be considered as consisting of three connected parts: a rippled region as a sample and two semi-infinite ideal regions as leads[23, 24]. The left and right leads can be assumed to be in equilibrium states with different chemical potentials  $\mu_L$  and  $\mu_R$ , respectively, where  $\mu_L - \mu_R$  is very small. Thus the current can be written as

$$j(\mathbf{r}, \mathbf{r}') = \frac{4}{h} \int_{\mu_R}^{\mu_L} \text{Re}[t(\mathbf{r} - \mathbf{r}') G^<(\mathbf{r}', \mathbf{r}, E)] dE, \quad (6)$$

where

$$G^< = G^r \Sigma_L^< G^a, \quad (7a)$$

$$G^{r,a} = (E^\pm I - H_c - \Sigma^{r,a})^{-1}, \quad (7b)$$

with  $E^\pm \equiv E \pm i0^+$  and  $H_c$  is the Hamiltonian matrix of the isolated sample.  $\Sigma^{r,a} = \Sigma_L^{r,a} + \Sigma_R^{r,a}$  is the self-energy arisen from the couplings between the sample and two leads.  $\Sigma_{L,R}^< = f_{L,R}(\Sigma_{R,L}^a - \Sigma_{R,L}^r)$ , where the Fermi functions  $f_{L,R}$  satisfy  $f_{L,R}(E) \simeq \theta(\mu_{L,R} - E)$  at low temperature.  $\Sigma_{R,L}^{r,a}$  can be obtained by using the iterative method developed by Lopez-Sancho et.al.[23]. To reduce the calculation and memory requirement, we orderly denote the layers of the sample from the left to the right by  $1, 2, \dots, l$ , thus the necessary sub-matrices  $G_{n,n-1}^<$  and  $G_{n,n}^<$  for calculating current can be obtained by following back-and-forth recurrence procedure:

$$g_{n,n}^{r,a} = (E^\pm I - H_{n,n} - \Sigma_{R,n}^{r,a})^{-1}, \quad (8a)$$

$$\Sigma_{R,n-1}^r = H_{n-1,n} g_{n,n}^r H_{n,n-1}, \quad (8b)$$

with  $n = l, \dots, 2$  and  $\Sigma_{R,l}^r = \Sigma_R^r$ . For  $\mu_R \leq E \leq \mu_L$ ,

$$G_{n,n-1}^< = g_{n,n}^r H_{n,n-1} G_{n-1,n-1}^<, \quad (9a)$$

$$G_{n,n}^< = G_{n,n-1}^< H_{n-1,n} g_{n,n}^a, \quad (9b)$$

with  $n = 2, \dots, l$  and  $G_{1,1}^< = G_{1,1}^r \Sigma_L^< G_{1,1}^a$ , where

$$G_{1,1}^{r,a} = [E^\pm I - H_{1,1} - \Sigma_{R,1}^{r,a} - \Sigma_{L,1}^{r,a}]^{-1}. \quad (10)$$

Similarly, the LDOS

$$\rho(\mathbf{r}, E) = \frac{1}{2\pi} A(\mathbf{r}, \mathbf{r}), \quad (11)$$

where  $A = i(G^r - G^a)$ , and the conductance

$$T(E) = \frac{2e^2}{h} \text{Tr}[\Gamma_R (A - G^r \Gamma_R G^a)], \quad (12)$$

with  $\Gamma_{R,L} = i(\Sigma_{R,L}^r - \Sigma_{R,L}^a)$ , can also be obtained by the same method.

In order to see the ripple's influence on the current as clear as possible, the inherent deflection due to the lattice background has to be averaged out. To this end we define a cell-average current as an average vector of six bond currents around a honeycomb cell

$$\mathbf{j}(\mathbf{r}_c) = \frac{1}{6} \sum_{i < j} j(\mathbf{r}_i, \mathbf{r}_j) \frac{\mathbf{r}_j - \mathbf{r}_i}{|\mathbf{r}_j - \mathbf{r}_i|}, \quad (13)$$

where  $\mathbf{r}_{i,j}$  denote the vertices of the cell,  $\mathbf{r}_c$  is the cell center.

### C. Results and Discussion

First we compare the LDOSs and conductances for a fixed GNR with different ripples. Fig.2 shows the LDOSs and conductances for a zigzag and an armchair GNR in the presence of different ripples given by Eq.(5) with different  $h$ 's and orientations (represented by slope angle  $\theta_{\mathbf{k}}$ ). The most remarkable change is that the conductance near every step edge of the conductance staircase is remarkably decreased. Meanwhile, each corresponding van Hove peak in LDOSs is also broaden and successively split into two sub-peaks when  $h$  reaches critical values, except for zigzag GNRs with  $\theta_{\mathbf{k}} = 0^\circ$  (which will be further discussed in the last paragraph). The critical degrees of deformation can be represented by the associated maximum relative bond elongation due to the ripple. This bond elongation can be roughly estimated from the ratio between the ripple's height  $h$  and wavelength  $\lambda$  if we consider only the atomic height fluctuation. For zigzag GNRs with  $\theta_{\mathbf{k}} = 30^\circ$ , this critical ratio is about  $1/20$ , the corresponding maximum relative bond elongation is about 5%.

To get an intuitive understanding of the microscopic behavior of electrons that gives rise to these changes, now we analyze the spatial distributions of the LDOS  $\rho(\mathbf{r}, E)$  and current  $\mathbf{j}(\mathbf{r}_c, E)$  at the corresponding energies. Fig.3 shows two examples of this kind of LDOS and current distributions in a rippled  $N = 20$  zigzag GNR at  $0.56\text{eV}$  and  $0.61\text{eV}$ , respectively corresponding to two

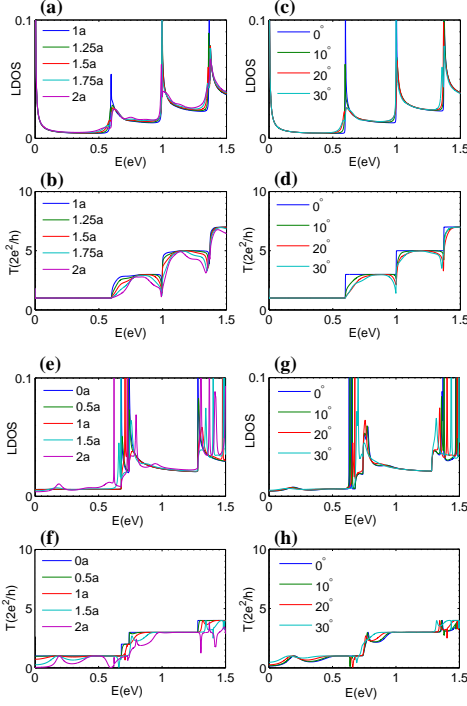


FIG. 2: (a) LDOS and (b) conductance of rippled  $N = 20$  zigzag GNRs as shown in Fig.1 for different  $h$ 's, where  $\lambda = 30a$ ,  $\theta_k = 30^\circ$ . (c) LDOS and (d) conductance of identical GNRs as Fig.1 for different  $\theta_k$ 's, where  $h = 1.5a$ ,  $\lambda = 30a$ . (e) LDOS and (f) conductance of  $N = 20$  armchair GNRs for different  $h$ 's, here  $\lambda = 40a$ ,  $\theta_k = 20^\circ$ . (g) LDOS and (h) conductance of identical GNRs as (e,f) for different  $\theta_k$ 's, where  $h = 1.5a$ ,  $\phi_0 = -\pi/2$ .

sub-peaks split off from the first van Hove peak in conducting sub-band. We can see from the LDOS distributions (Fig.3(a,c)) that the lower sub-peak is mainly localized in the ripple area; while the upper one (belonging to the bottom of the first conducting sub-band) is extended, its LDOS does not decay outside the ripple region. More importantly, their current distributions both occur remarkable vortices (Fig.3(b,d)). Some current lines even form closed loops, showing that these currents are not potential flow. Similarly, the second van Hove peak also splits into two sub-peaks and their current distributions also have this vortical feature. The valence bands also occur identical phenomena. When the bias is reversed, these eddy currents will also be exactly reversed, thus an alternative bias can drive a varying eddy current in this kind of rippled GNRs.

At first sight, these vortices seems can be ascribed to Landau-like quasi-bound states caused by the ripple-induced pseudo-magnetic field, since according to the continuous model a geometrical deformation will induce an effective vector potential

$$\mathbf{A} \simeq \frac{1}{2}(\sqrt{3}(t_3 - t_2), t_3 + t_2 - 2t_1) \quad (14)$$

with  $t_{1,2,3}$  three nearest hopping amplitudes[15]. Actu-

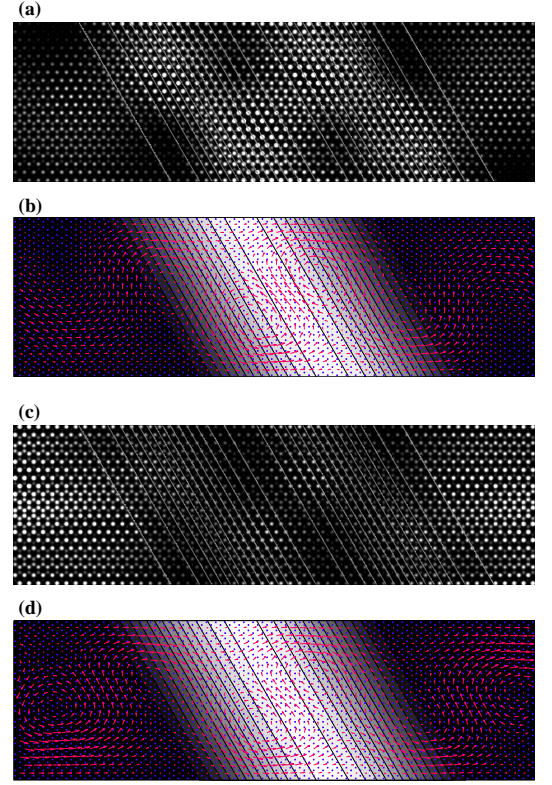


FIG. 3: (a) LDOS and (b) current distribution at 0.56eV (the lower sub-peak split off from 1st van Hove peak) in an  $N = 20$  zigzag GNR as shown in Fig.1. (c) LDOS and (d) current at 0.61eV (the upper sub-peak of the 1st van Hove peak) in the same GNR. The brightness in (a,c) represents the LDOS, the contours depict the ripple. The brightness in (b,d) represents the height of the ripple.

ally, some conductance fluctuation phenomena similar to the results shown in Fig.(2) have been observed in the measurement of differential conductance of graphene sheet with nanobubbles, and the researchers interpreted all this conductance fluctuation as the contribution of the Landau levels arising from the pseudo-magnetic field[11]. It is true that most of the above results can be explained by this pseudo-magnetic field. For example, if  $\mathbf{k}$  is exactly along some special directions, e.g.,  $\theta_k = 0^\circ, 30^\circ, 60^\circ$ , we can deduce some general properties of  $\mathbf{A}$  by qualitative analysis, which can be compared with the numerical results. In these special cases the  $\mathbf{A}$  will have the form  $\mathbf{A}_0 \cos(\mathbf{k} \cdot \mathbf{r} + \phi_0)$  and will be parallel or perpendicular to  $\mathbf{k}$ [16]. More specifically, for rippled zigzag GNRs of  $\theta_k = 0^\circ, 60^\circ$  or armchair GNRs of  $\theta_k = 30^\circ$ ,  $\mathbf{A}$  is nearly parallel to  $\mathbf{k}$ , so the pseudo-magnetic field  $\nabla \times \mathbf{A} \simeq -\mathbf{k} \times \mathbf{A}_0 \sin(\mathbf{k} \cdot \mathbf{r} + \phi_0)$  is very small, thus the ripple influence will be much weaker than other ripple orientations; while for armchair GNRs of  $\theta_k = 0^\circ$  or zigzag GNRs of  $\theta_k = 30^\circ$ ,  $\mathbf{A}$  is perpendicular to  $\mathbf{k}$ , so the pseudo-magnetic field is strong and will strongly disturb the electronic states. For these special cases, the above

explanation is qualitatively in accord with the result in Fig.2 (there are still some more subtle problems, which will be discussed in last paragraph).

However, these current distributions also exhibit a remarkable feature revealing that this is not the whole story. We notice that if the energy slightly higher than the bottom of a conducting sub-band (or lower than the top of a valance sub-band), the vortices of the eddy current will not entirely lie within the ripple region, but also occur in flat regions far from the ripple, where the pseudo-magnetic field has vanished, as can be seen from Fig.3(d). This feature reveals that these vortices cannot be interpreted as Landau states produced by the pseudo-magnetic field, because all ripple-induced scattering mechanisms, both the pseudo-magnetic field and the velocity variation, only act locally within the ripple area, hence the electronic waves should freely propagate in flat areas. Fig.4(a,b) give other two examples of this global

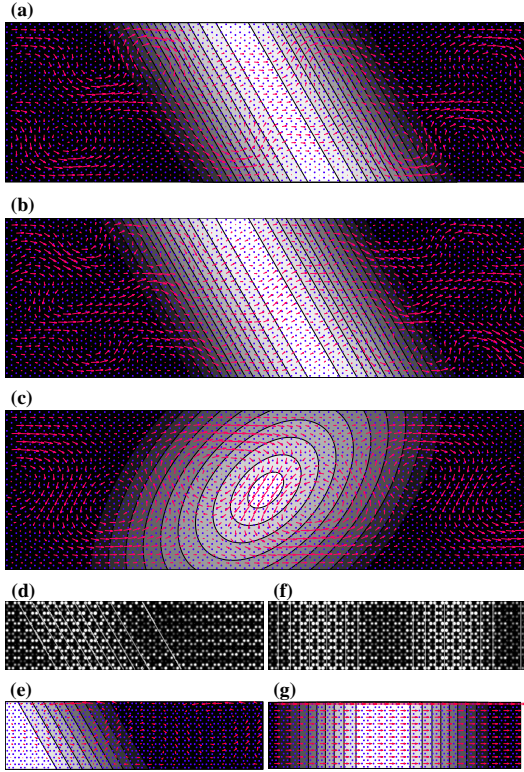


FIG. 4: (a) Eddy current in the same GNR as Fig.1 at 1eV, the upper sub-peak of the second van Hove peak, and (b) 1.37eV, the upper sub-peak of the third van Hove peak. (c) Eddy current at 0.6eV in a similar GNR as Fig.3(c,d) but with a hyperbolic-surface ripple given by Eq.(15). (d) LDOS and (e) current distribution at 0.69eV in an  $N = 20$  armchair GNR with a ripple given by Eq.(5), where  $h = 1.5a$ ,  $\lambda = 40a$ ,  $\theta_{\mathbf{k}} = 30^\circ$ ,  $\phi_0 = -\pi/2$ . (f) LDOS and (g) current distribution at 0.631eV in a GNR as (d,e) except  $\theta_{\mathbf{k}} = 0^\circ$ .

eddy currents in the same zigzag GNR as Fig.3, their energies are slightly above the second and third van Hove peaks of the conducting band, respectively. We can see

that both of them have pronounced vortices in the flat areas far beyond the ripple, where the pseudo-magnetic field has certainly vanished. Generally, if the ripple is slope relative to the GNR axis, the current distributions within the energy range slightly above the bottom of a conducting sub-band or below the top of a valance sub-band will occur remarkable vortices in entire flat areas. These vortices appeared in flat areas are rather exotic because there is no local responsible deflection mechanism.

In order to explain the origin of these exotic vortices, we have to notice two basic properties of the electronic states of GNRs under perturbation. The first is that the electronic states will become superposition of partial waves with approximate energies. The second is that the velocity direction (forward or backward relative to GNR's axis) of the states near the bottom of a conducting sub-band (or the top of a valance sub-band) is unstable, because its velocity  $\partial E(\mathbf{k})/\partial k_x$  ( $k_x$  is the momentum component along the GNR axis) is very small, so its sign can be easily changed by a small variation of  $E(\mathbf{k})$ , as illustrated in Fig.5(a,b). Therefore, if there is a nonuni-

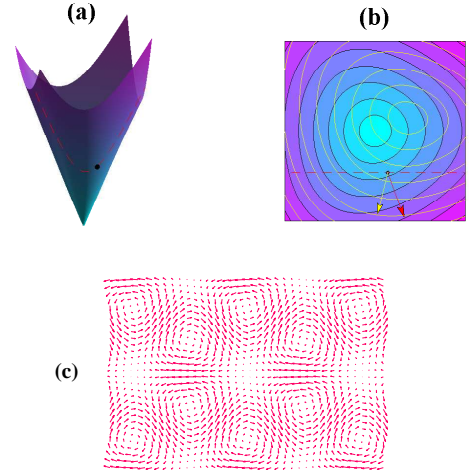


FIG. 5: (a) Conducting band of graphene near a Fermi point, the red dashed line represents a sub-band of a GNR. The velocity of states near the minimum of the sub-band (red dashed line) can be easily reversed under a small variation of the energy band, as shown in (b). (b) Contour map of energy bands for a perfect (blue-purple) and a deformed (yellow) graphene. For the deformed one, only two bonds are elongated respectively by 5.3% and 2.8%. The red(yellow) arrow represents the velocities of a state in perfect(deformed) graphene. (c) Current distribution of three plane waves.

form deformation, the perturbed state corresponding to an originally forward state in these energy ranges may contribute a backward flow in the deformed regions. In particular, this local backward flow demands the perturbed state to include backward partial waves in flat areas in order to satisfy continuity condition at the interfaces between deformed and flat areas, though there exists no local responsible scattering mechanism. These



partial waves of different directions are always spatially superimposed due to the edge reflection and will produce interference. Consequently, the current density no longer equals to the sum of the currents of every partial waves,  $\mathbf{j}(\mathbf{r}) \neq \sum \langle \mathbf{k} | \mathbf{j}(\mathbf{r}) | \mathbf{k} \rangle$ , but must include interference terms  $\langle \mathbf{k} | \mathbf{j}(\mathbf{r}) | \mathbf{k}' \rangle$ , similar to the usual interference for probability density. These kind of current interference patterns will be winding or eddying flows in areas without any local deflection mechanism. As a simplest example, Fig.5(c) shows the current interference pattern of three plane waves  $\psi(\mathbf{r}) = e^{i\mathbf{k}_1 \cdot \mathbf{r}} + e^{i\mathbf{k}_2 \cdot \mathbf{r}} + e^{i\mathbf{k}_3 \cdot \mathbf{r}}$ , where  $\mathbf{k}_{1,2,3}$  have equal length while their included angles are  $120^\circ$ . We can see that its current distribution forms a very similar eddying pattern. Obviously, the vortex scale of these eddy currents arising from the interference is in proportional to the wavelengths of the partial waves. For the eddy currents in rippled GNRs, this character can also be verified by comparing Fig.3(a,d) and Fig.4(a,b). We find that the vortices become smaller and smaller with the increasing of energy owing to the linear dispersion relation  $E \propto k$ . Conversely, the vortex scale will be very large in wider GNRs because the energies of each corresponding step of the conductance staircases will be smaller, it is only limited by the electronic interference length.

According to this explanation, these global eddy currents would be a rather ubiquitous effect in rippled GNRs, although their patterns depend on specific ripple configurations. Fig.4(c) is another eddy current in an identical zigzag GNR in the same energy range as Fig.3(b) but with different ripples, which is a hyperbolic surface

$$z(\mathbf{r}) = \begin{cases} h[1 - f(\mathbf{r})], & f(\mathbf{r}) \leq 1 \\ 0, & f(\mathbf{r}) > 1, \end{cases} \quad (15)$$

where  $f(\mathbf{r}) = \sqrt{\left(\frac{\hat{\mathbf{e}}_1 \cdot \mathbf{r}}{a_0}\right)^2 + \left(\frac{\hat{\mathbf{e}}_2 \cdot \mathbf{r}}{b_0}\right)^2}$ , with  $h = 4a$ ,  $a_0 = 15a$ ,  $b_0 = 25a$ ,  $\hat{\mathbf{e}}_{1,2} = (\sqrt{2}/2, \mp\sqrt{2}/2)$  (its maximum bond elongation is about 3%). By comparing Fig.3(d) and Fig.4(c), we can see that their current distributions in flat regions are very similar although their ripple are very different. Similar to this structural insensitivity of the global eddying character, it is conceivable from the above explanation that this vortical character will also not very sensitive to the energy variation. Actually, the representation of these eddying states in the LDOS curve is not a sharp peak like quasi-bound states, but a broad and smooth one forming a piece of continuous spectrum (Fig.2).

In addition, there are few special cases worth to be particularly pointed out. The first case is zigzag GNRs with  $\theta_{\mathbf{k}} = 0^\circ$ . In this case the current lines remain to be straight lines and no vortex occurs, because in this case the  $\mathbf{A}$  is parallel to  $\mathbf{k}$  according Eq.(14) or [16], so the  $\nabla \times \mathbf{A}$  can be ignored; moreover, the incident current is along a symmetric axis of the energy band, so the refraction also does not change its direction. The second is zigzag GNRs with  $\theta_{\mathbf{k}} = \pm 60^\circ$  or armchairs GNRs with  $\theta_{\mathbf{k}} = \pm 30^\circ$ . Similar to the first case, here the  $\nabla \times \mathbf{A}$  are also very small, however, there exist apparent vortices, as shown in Fig.4(e), because in these cases the anisotropic deformation of the energy contours (see Fig.5(b)) will result in similar backward flow. The third one is armchair GNRs of  $\theta_{\mathbf{k}} = 0^\circ$ , although the ripple induce a strong pseudo-magnetic field and results in apparent quasi-bound states (Fig.2(f) and Fig.4(f)), but their currents do not occur any vortex (Fig.4(g)), because the direction of the incident current is the symmetric axis of two pseudo-magnetic fields for two inequivalent Dirac points (mutually symmetric) as well as the principle axis of the velocity tensor, so the action of the pseudo-magnetic fields of two Dirac points will be mutually canceled out and the refraction and dispersion due to the velocity anisotropy also does not change the current direction.

In summary, the current flows near every step edge of the conductance staircases of a GNR are rather unstable. They will become eddy currents if there occurs a slope ripple. These eddy currents can be divided into two classes. The first one are carried by Landau-like states caused by the pseudo-magnetic field, these states have slightly lower energies and their current distributions form vortices only within the ripple region. In contrast, the second one are carried by some special scattering states, which have slightly higher energies and include backward partial waves in flat areas. Consequently, they will form some global eddy currents due to the interference of these partial waves. This global eddy current is a manifestation of the non-locality of quantum interference effect.

## Acknowledgments

This work was supported by "the Fundamental Research Funds for the Central Universities" and NSFC (Grant Nos. 10974027, 50832001).

- 
- [1] Novoselov K S, Geim A K, Morozov S V, Jiang D, Zhang Y, Dubonos S V, Grigorieva I V, and Firsov A A 2004 Electric Field Effect in Atomically Thin Carbon Films *Science* **306**, 666.
  - [2] Novoselov K S, Jiang D, Schedin F, Booth T J, Khotkevich V V, Morozov S M, and Geim A K 2005 wo-

dimensional atomic crystals *Proc. Natl. Acad. Sci.* **102**, 10451.

- [3] Novoselov K S, Geim K S, Morozov A K, Jiang D, Katsnelson M I, Grigorieva I V, Dobonos S V and Firsov A A 2005 Two-dimensional gas of massless Dirac fermions in graphene *Nature* **438**, 197-200.

- [4] Zhang Y, Tan Y W, Stormer H L and Kim P, 2005 Experimental observation of the quantum Hall effect and Berry's phase in graphene *Nature* **438**, 201-204.
- [5] Castro Neto A H, Guinea F, Peres N M R, Novoselov K S and Geim A K 2009 The electronic properties of graphene *Rev. Mod. Phys.* **81**, 109-162.
- [6] Meyer J C, Geim A K, Katsnelson M I, Novoselov K S, Booth T J and Roth S 2007 The structure of suspended graphene sheets *Nature* **446**, 60.
- [7] Vázquez de Parga A L, Calleja F, Borca B, Passeggi M C G, Jr. Hinarejos J J, Guinea F and Miranda R 2008 Periodically rippled graphene: Growth and spatially resolved electronic structure *Phys. Rev. Lett.* **100**, 056807.
- [8] Bao W, Miao F, Chen Z, Zhang H, Jang W, Dames C, and Lau C N 2009 Controlled ripple texturing of suspended graphene and ultrathin graphene membranes, *Nature nanotechnol.* **4**, 562-566.
- [9] de Juan F, Cortijo A, Vozmediano M A H 2007 Charge inhomogeneities due to smooth ripples in graphene sheets *Phys. Rev. B* **76**, 165409.
- [10] Guinea F, Katsnelson M I and Geim A K 2009 Energy gaps and a zero-field quantum Hall effect in graphene by strain engineering *Nature Phys.* **6**, 30-33.
- [11] Levy N, Burke S A, Meaker K L, Panlasigui M, Zettl A, Guinea F, Castro Neto A H and Crommie M F 2010 Strain-induced pseudo-magnetic fields greater than 300 Tesla in graphene nanobubbles, *Science* **329**, 544.
- [12] de Juan F, Cortijo A, Vozmediano M A H and Cano A 2011 Aharonov-Bohm interferences from local deformations in graphene *Nature Phys.* **7**, 810.
- [13] Suzuura H and Ando T 2002 Phonons and electron-phonon scattering in carbon nanotubes *Phys. Rev. B* **65**, 235412.
- [14] Mañes J L 2007 Symmetry-based approach to electron-phonon interactions in graphene, *Phys. Rev. B* **76**, 045430.
- [15] Vozmediano M A H, Katsnelson M I and Guinea F 2010 Gauge fields in graphene *Phys. Rep.* **496**, 109.
- [16] Yang H T 2011 Strain induced shift of Dirac points and the pseudo-magnetic field in graphene *J. Phys. Condens. Matt.* **23**, 505502.
- [17] Kadanoff L P and Baym G 1962, *Quantum Statistical Mechanics*, Benjamin, New York.
- [18] Keldysh L V 1965 Diagram technique for nonequilibrium processes *Sov. Phys. JETP.* **20**, 1018.
- [19] Chou K C, Su Z B, Hao B L and Yu L 1985 Equilibrium and nonequilibrium formalisms made unified *Phys. Rep.* **118**, 1-131.
- [20] Pereira V M, Castro Neto A H and Peres N M R 2009 Tight-binding approach to uniaxial strain in graphene, *Phys. Rev. B* **80**, 045401.
- [21] Pellegrino F M D, Angilella G G N and Pucci R 2010 Strain effect on the optical conductivity of graphene *Phys. Rev. B* **81**, 035411.
- [22] Areshkin D A and White C T 2007 Ballistic transport in graphene nanostrips in the presence of disorder: Importance of edge effects *Nano Lett.* **7**, 3253-3259.
- [23] Lopez-Sancho M P, Lopez-Sancho J M and Rubio J 1984 Highly convergent schemes for the calculation of bulk and surface Green functions *J. Phys. F* **14**, 1205.
- [24] Lake R, Klimeck G, Bowen R C and Jovanovic D 1997 Single and multiband modeling of quantum electron transport through layered semiconductor devices *J. Appl. Phys.* **81**, 7845.